JOURNAL OF SOLID STATE CHEMISTRY **136,** 233–246 (1998)
ARTICLE NO. SC977688

Determination of Structure Candidates of Simple Crystalline AB_2 Systems

M. A. C. Wevers, J. C. Schön,[1] and M. Jansen

Institut für Anorganische Chemie, Universität Bonn, Gerhardt-Domagk-Strasse 1, D-53121 Bonn, Germany

Received June 6, 1997; in revised form October 17, 1997; accepted October 27, 1997

The potential energy surface of the fluorides and chlorides of magnesium and calcium is studied using a global optimization method (simulated annealing). Emerging configurations exhibit a structure variance very similar to that of real crystalline AB_2 systems. The local minima suggest new possible structure types in AB_2 systems. The influence of the variation of potential parameters on the resulting configurations is investigated and discussed. © 1998 Academic Press

Key Words: **alkaline-earth halides; simulated annealing; structure prediction; potential energy surface.**

1. INTRODUCTION

The crystal structure is the key to understanding the electronic and chemical properties of solid state compounds (1, 2). A promising approach toward the prediction of the emerging crystal structures of solid state reactions is the investigation of the energy landscapes of hypothetical compounds with competing minimum structures. Once the local minima on the energy hypersurface are known, finding chemical systems with stable modifications and finally planning synthesis routes for such compounds appear to be possible (3).

If global optimization methods are employed, the use of simple empirical potentials is essential because energy calculations on the ab initio level are still computationally very expensive (4). In particular, since no information about crystallographic cell constants is available, the configuration space that needs to be investigated is greatly enlarged due to the necessary variation of the simulation cell compared to only an adjustment of atomic coordinates. This enforces a trade-off between the speed and the accuracy of the energy calculation. In such a case, the global optimization requires appropriate approximate energy functions. The resulting local minima are structure candidates that can serve as initial configurations for further investigations with more sophisticated energy calculations such as the LDA (5) or Hartree–Fock approach (6). Furthermore, a thermodynamic stability analysis of these hypothetical structures can be performed (3, 7, 8) using algorithms that provide knowledge of the energy barriers around these minima and the local density of states near the minima (9, 10).

In related work, global optimization of cost functions consisting of a sum of the potential energy and various penalty terms has been performed for systems where certain chemical information was already available (11–14). Such attempts at determining crystal structures based on experimental data, e.g., cell constants, using simulated annealing methods have been encouragingly successful (15–17). However, such cost functions are usually not suitable for hypothetical solid compounds that are expected to exhibit a (meta)stable crystalline structure but have not yet been synthesized, as for example Na_3N (3). Since our goal is the prediction of the structures of such not-yet-synthesized compounds, we use only empirical potentials to approximate the energy function. Earlier results in simple ionic A_xB_y systems indicate that the real crystal structures are well represented by an empirical potential that is used for the energy calculations with relatively low computational cost (3, 18). In this study, the energy landscapes of alkaline-earth fluorides and chlorides of magnesium and calcium are investigated.

2. POTENTIAL

The energy function used for calculating the potential energy is a combined Coulomb and Lennard-Jones potential for ionic crystals. The long-range forces are calculated by Ewald summation in the formulation of De Leeuw *et al.* (19). The repulsion between neighboring ions is controlled by the r^{-12} term in the Lennard-Jones part while the attraction due to the polarization of the ions is expressed by the van der Waals r^{-6} term. Thus, the energy function for N atoms takes the form

$$E = E_{\text{total}}/N = E_{\text{Coulomb}}/N + E_{\text{Lennard-Jones}}/N \quad \text{(units: eV/atom)}, \qquad [1]$$

[1]To whom correspondence should be addressed.

0022-4596/98 $25.00

where

$$E_{\text{Lennard-Jones}} = \frac{1}{2}\sum_{i\neq j}^{N}\left(\varepsilon\left[\left(\frac{\sigma_{ij}}{r_{ij}}\right)^{6} - \left(\frac{\sigma_{ij}}{r_{ij}}\right)^{12}\right]\right),$$
$$\text{with } \sigma_{ij} = (R_i + R_j)r_s \qquad [2a]$$

and

$$E_{\text{Coulomb}} = \sum_{i=1}^{N}\sum_{j<i}^{N} q_i q_j \Psi(\mathbf{r}_{ij}) + \frac{1}{2}\xi\sum_{i=1}^{N} q_i^2 + \frac{2\pi}{3}\left|\sum_{i=1}^{N} q_i \mathbf{x}_i\right|^2, \qquad [2b]$$

with

$$\Psi(\mathbf{r}_{ij}) = \sum_{\mathbf{n}}\left(\frac{\operatorname{erfc}(\alpha\cdot|\mathbf{r}_{ij}+\mathbf{n}|)}{|\mathbf{r}_{ij}+\mathbf{n}|}\right) + \sum_{k}{}'\left|\frac{e^{-(\pi^2\mathbf{h}_k^2\alpha^{-2} + 2\pi i(\mathbf{h}_k\cdot\mathbf{r}_{ij}))}}{\pi V_0 \mathbf{h}_k^2}\right| \qquad [3a]$$

and

$$\xi = \sum_{k}{}'\left(\frac{\operatorname{erfc}(\alpha\cdot|\mathbf{n}|)}{|\mathbf{n}|} + \frac{e^{-(\pi^2\mathbf{h}_k^2\alpha^{-2})}}{\pi V_0 \mathbf{h}_k^2}\right) - \frac{2\alpha}{\sqrt{\pi}}. \qquad [3b]$$

Here, α denotes the convergence parameter of the Ewald summation, which is adjusted during the optimization for every cell change in such a way that all terms are included that are not lower than a fixed value determined by the prescribed accuracy of the energy calculation (20). In our case the total energy is calculated with a precision of 10^{-3} eV/atom. $\mathbf{r}_{ij}$ is the vector between ions i and j, and $\mathbf{x}_i$ is the position of ion i in the simulation cell with the volume V_0. $\mathbf{n}$ denotes a direct lattice vector, and $\mathbf{h}_k$ is a reciprocal lattice vector. A prime on the summation sign indicates that the zero vector is excluded from the summation. The radius of the ion i is R_i, and the Lennard-Jones parameter is ε.

The Lennard-Jones potential contributes usually about 10% of the total energy (21), and the order of magnitude for ε has been chosen accordingly. The parameters ε and r_s in the potential have not been fitted to experimental values, because the necessary data are not available for every relevant configuration. Instead the parameters are usually varied in a relatively wide range of physically reasonable values in order to study their influence on the resulting energy landscape (18).

The ionic radii in the sum $\sigma_{ij} = (R_i + R_j)r_s$ are scaled by altering the parameter r_s in the Lennard-Jones part of the potential. The ionic radii were taken from the literature (22) (see Table 1). In contrast to Shannon radii, these effective radii have the advantage that they are averaged over different coordination numbers. The charge was always the formal charge of the ion corresponding to the point charge model for lattice energy calculations. To reduce the number of empirical parameters as much as possible, r_s was set equal to 1.0. For the same reason, the Lennard-Jones parameter ε was chosen to be independent of the ion types. In this work ε is changed for each different set of optimization runs ($0.1 < \varepsilon < 0.5$ in the standard simulated annealing runs). It should be noted that the ions present in the system are only characterized by the ionic charge and the ionic radii in the potential.

TABLE 1

Cation, Anion $R_{\text{cation}}/R_{\text{anion}}$, and Mean Cation–Anion Distances (d_{mean}) for Each Combination of the Ions Mg^{2+}, Ca^{2+}, F^-, and Cl^- [a]

Ion	$\sigma_{\text{cation, anion}}$ (pm)	$R_{\text{cation}}/R_{\text{anion}}$	d_{mean} (Å)
Mg	211 (F)	0.586 (F)	1.99 (F)
	259 (Cl)	0.431 (Cl)	2.33 (Cl)
Ca	239 (F)	0.809 (F)	2.36 (F)
	287 (Cl)	0.586 (Cl)	2.73 (Cl)

[a] The effective ionic radii R_i for Mg^{2+}, Ca^{2+}, F^-, and Cl^- used in the Lennard–Jones potential are 78, 106, 133, and 181 pm, respectively. The resulting σ_{ij} parameter for each cation–anion combination, the radius ratio for these values, and the mean cation–anion distance d_{mean} measured in the crystal (34) are given in the table.

3. OPTIMIZATION METHOD

The determination of structure candidates is carried out using a standard simulated annealing algorithm (23) with the potential energy based on an empirical potential as the cost function. Starting from different random atomic configurations, the cell parameters and the atomic coordinates are varied stochastically according to a move class (random walk). To handle the large number of atoms (10^{23}) in a macroscopic crystalline system, periodic boundary conditions are applied.

The system's probability for accepting a change of the configuration in the case of a rise in energy is given by the Metropolis criterion (24). This is based on an exponential expression of the form $f_C(\Delta E) = e^{-\Delta E/C}$, where ΔE is the energy difference of the configuration with and without the calculated change and the control parameter C resembles the temperature in a real annealing process. The move is allowed if a random number between zero and one is lower than $f_C(\Delta E)$. By reducing C during the optimization according to a temperature schedule, the probability for crossing an energy barrier decreases with optimization time, so that, at the end of a run, almost only energy lowering moves are allowed (quench phase). The resulting configuration should be in or at least very close to a local minimum on the energy hypersurface. Subsequently applying local optimization methods such as gradient or quench algorithms should bring the system completely to the local minimum (25).

In the present work, random atomic configurations in a simulation cell (periodic boundary conditions) with more

than three times the volume of the ions were chosen as starting points. The simulation cell for an AB_2 system has usually been chosen to contain six atoms (number of formula units: $Z = 2$). For comparison, optimizations with $Z = 4$ have also been performed. In the discussion these results will be briefly reported.

Since we are interested in scanning the multiminima landscape, to determine as many structure candidates as possible, it is advantageous to perform relatively short runs with many different random walk sequences. Every 100 steps the control parameter C was reduced according to a hyperbolic temperature schedule ($C(n) = C(0) \cdot d^n$, where n = number of updates; here $d = 0.992$ and $C(0) = 0.1$ eV). For the MgF_2 system the number of steps between the C updates was 200. The number of C updates was 1000 for each complete optimization run.[2] A set of 20 simulated annealing runs with different random numbers was performed for the A_2B_4 combinations of A = Mg or Ca and B = Cl or F for each value of ε.

The move class employed in this study is based on previous work (7, 18, 26). It comprises 80% change of atom coordinates, 5% atom exchange, cell vector change with (5%)/without (5%) changing relative atom positions, and 5% adding a slice to or subtracting a slice from the cell. Since preliminary simulated annealing runs have established that the preferred ionic charges are Mg^{2+}, Ca^{2+}, F^-, and Cl^-, no moves that change the charge of the ions need to be included (18). The size of the change is coupled with the temperature program reducing the size of the steps toward the end of the simulated annealing.

4. OPTIMIZATION RESULTS

Most of the end configurations of the simulated annealing runs were close to local minima, indicated by their clearly defined coordination sphere about the cations and the small energy distribution for each of the different structures (about 0.005–0.001 eV/atom for undistorted structures). These clearly distinguishable minima showed mostly real crystal structure types. However, in some cases (less than 2%) additional local optimizations were necessary to obtain a configuration that is in the close neighborhood of a minimum. Such end configurations of simulated annealing runs typically had high energies and no distinct coordination sphere.

4.1. Minima

The simulated annealing end configurations are listed in Table 2. They are classified according to the coordination number (CN) of cations surrounded by nearest-neighbor anions and the name of the structure type that corresponds to the particular connection between the idealized polyhedra. Structures of minima that cannot be associated with existing crystal structure types and occur at least at three different ε values are discussed separately. The minimum for MgF_2 corresponding to the (distorted) anatase type has also been included. The crystallographic information for these minima as listed in Table 3 has been determined by applying a space group detection program[3] (27). End configurations without either of these characteristics are summarized in "other" minima (F) in Table 2.

The distribution of coordination numbers is in agreement with the radius ratio rule. For all systems the coordination number six is the most common one except for CaF_2, where the radius ratio rule predicts CN = 8. Only for the system $MgCl_2$, where the radius ratio is smallest, is the coordination number four significant; i.e., relatively deep-lying minima with CN = 4 exist. Only a slight ε dependence of the distribution over the possible coordination numbers in the local minima is observed. The tendency to form structures with higher coordination numbers (i.e., CN = 6 vs CN = 4, CN = 8 vs CN = 6) upon an increase in ε is largest in the $MgCl_2$ and CaF_2 systems. However, this may not be a general tendency in all cases. For example, in $CaCl_2$ the number of occurrences of the rutile-like structure increases at the expense of the number of sevenfold-coordinated MP1 structures. These observations could be quantified by improved statistics.[4]

4.2. End Configurations with New Structures

The coordination number seven appears in all systems except $MgCl_2$. The corresponding structures consist of monocapped trigonal prisms. In Fig. 1c a ball-and-stick representation of the minimum structure B1 is drawn. The monocapped prisms are connected by corners and edges only with the prism caps facing the same direction. The similarity to the fourfold-coordinated E1-structure becomes obvious upon analyzing some slightly distorted end configurations with a (4 + 3) coordination (see Fig. 1).

In the B2 minimum structure that occurs in CaF_2 the monocapped prisms are connected by edges and triangular faces of the prism and pyramidal parts of the polyhedron in a zigzag fashion pointing in different directions.

In contrast to other sevenfold-coordinated structures, as often found in numerous alkaline-earth or lanthanide

[2] On an HP-9000/735-125 machine one complete set of 20 runs with a total of 10^5 optimization steps each takes about 2800 min of CPU time.

[3] It should be noted that in order to find the highest possible symmetries in these structures some idealizations have to be made (i.e., putting atoms in special positions if the deviation is small). For some minima this results in a larger separation of the nearest-neighbor distances and a splitting of the coordination sphere. For example, a sixfold octahedral coordination may become an elongated 4 + 2 octahedral coordination.

[4] Such an in-depth study would require, in addition, the analysis of the influence of the temperature schedule of the simulated annealing on this distribution.

TABLE 2
Number of Occurrences of End Configurations for Different ε Values Classified by Coordination Number (CN) and the Name of the Corresponding Structure Type in the AB_2 Systems MgF_2, $MgCl_2$, CaF_2, and $CaCl_2$ ($Z = 2$)

$\varepsilon(Mg_2F_4)$	A (CN = 8) A1, A2	B (CN = 7) B1, B2	C (CN = 6) C1, C2, C3, C4, C5	D (CN = 5) D1, D2	E (CN = 4) E1, E2, E3, E4	F (other) F1, F2, F3
0.1	0, 0	0, 0	5, 1, 5, 2, 1	1, 1	0, 0, 0, 0	1, 3, 0
0.2	0, 0	6, 0	9, 2, 2, 0, 0	0, 1	0, 0, 0, 0	0, 0, 0
0.3	0, 0	7, 0	8, 2, 2, 0, 0	0, 1	0, 0, 0, 0	0, 0, 0
0.4	0, 0	4, 0	8, 1, 5, 1, 1	0, 0	0, 0, 0, 0	0, 0, 0
0.5	0, 0	4, 0	8, 1, 6, 0, 0	0, 0	0, 0, 0, 0	1, 0, 0
$\varepsilon(Mg_2Cl_4)$	A (CN = 8) A1, A2	B (CN = 7) B1, B2	C (CN = 6) C1, C2, C3, C4, C5	D (CN = 5) D1, D2	E (CN = 4) E1, E2	F (other) F1, F2, F3
0.1	0, 0	0, 0	3, 0, 0, 0, 0	0, 0	7, 4, 1, 5	0, 0, 0
0.2	0, 0	0, 0	11, 0, 2, 0, 0	0, 0	2, 1, 2, 1	0, 0, 1
0.3	0, 0	0, 0	7, 4, 1, 0, 0	1, 0	0, 4, 1, 0	1, 0, 1
0.4	0, 0	0, 0	14, 2, 1, 0, 0	0, 0	0, 0, 1, 0	0, 0, 2
0.5	0, 0	0, 0	10, 6, 1, 0, 0	0, 0	2, 0, 0, 0	0, 0, 1
$\varepsilon(Ca_2F_4)$	A (CN = 8) A1, A2	B (CN = 7) B1, B2	C (CN = 6) C1, C2, C3, C4, C5	D (CN = 5) D1, D2	E (CN = 4) E1, E2	F (other) F1, F2, F3
0.1	7, 1	0, 1	3, 0, 4, 0, 0	0, 0	0, 0, 0, 0	2, 3, 0
0.2	13, 0	1, 1	3, 0, 1, 0, 0	0, 0	0, 0, 0, 0	1, 0, 0
0.3	15, 0	2, 1	0, 0, 0, 0, 0	0, 0	0, 0, 0, 0	0, 2, 0
0.4	15, 1	2, 0	0, 0, 0, 0, 0	0, 0	0, 0, 0, 0	2, 0, 0
0.5	14, 0	2, 0	2, 0, 0, 0, 0	0, 0	0, 0, 0, 0	2, 0, 0
$\varepsilon(Ca_2Cl_4)$	A (CN = 8) A1, A2	B (CN = 7) B1, B2	C (CN = 6) C1, C2, C3, C4, C5	D (CN = 5) D1, D2	E (CN = 4) E1, E2	F (other) F1, F2, F3
0.1	0, 0	7, 0	4, 0, 4, 0, 0	0, 0	0, 0, 0, 0	0, 3, 2
0.2	0, 0	4, 0	6, 3, 4, 1, 0	0, 0	0, 0, 0, 0	1, 0, 1
0.3	0, 0	1, 0	12, 3, 2, 0, 0	0, 0	0, 0, 0, 0	0, 2, 0
0.4	0, 0	5, 0	9, 3, 2, 1, 0	0, 0	0, 0, 0, 0	0, 0, 0
0.5	0, 0	8, 0	9, 2, 0, 1, 0	0, 0	0, 0, 0, 0	0, 0, 0

A (CN = 8):	A1	fluorite type
	A2	"cubes" (edge- and face-connected quadratic prisms)
B (CN = 7):	B1	monocapped prisms (edge-to-corner-connected prisms), MP1
	B2	monocapped prisms (edge-to-edge-connected prisms), MP2
C (CN = 6):	C1	rutile type
	C2	half-filled NaCl type (edge- and corner-connected octahedra); cubic close packing of anions with half-filled octahedral sites, arranged in corner-connected layers, "ccp, $\frac{1}{2}$O" (cf. ReO_3-type (see also Fig. 2))
	C3	CdI_2 type
	C4	"prisms" (edge- and corner-connected)
	C5	anatase type (distorted)
D (CN = 5):	D1	trigonal bipyramids; sheets of halffilled ionic boron nitride structure, BiPy1
	D2	trigonal bipyramids, six-membered rings, BiPy2
E (CN = 4):	E1	layers of corner-connected chains of alternating edge-connected tetrahedra
	E2	HgI_2-like (26) layers of corner-connected identically orientated tetrahedra
	E3	layers of six-membered rings of alternating tetrahedra connected by corners
	E4	corner-connected orthogonal chains of corner-connected tetrahedra equally orientated
F (other):	F1	very distorted structures or no clearly defined coordination
	F2	different structures (single) or mixture of different distinct polyhedra
	F3	special case of F2: intermediate between E1 and C2

TABLE 3
Crystallographic Data (Space Groups, Crystal Systems, Cell Constants, and Atomic Positions) for the (Idealized) New Minimum Structures (Classified According to Table 2) for the Corresponding AB_2 Systems

(Minimum), AB_2 system	Space group (number), special choice, crystal system	Cell constants [a, b, c (Å), α, β, γ (deg)]	Atom (multiplicity, Wyckoff letter), positional coordinates			
			atom	x	y	z
(A2), CaF_2	$P4/mmm$ (123), tetragonal	$a = 3.735, b = 3.735, c = 2.867$	Ca (1*b*)	0	0	$\frac{1}{2}$
		$\alpha = 90.00, \beta = 90.00, \gamma = 90.00$	F (2*f*)	0	$\frac{1}{2}$	0
(B1), $CaCl_2$	$Pmn2_1$ (31), orthorhombic	$a = 4.524, b = 6.900, c = 5.172$	Ca (4*b*)	$\frac{1}{2}$	0.572	0.650
		$\alpha = 90.00, \beta = 90.00, \gamma = 90.00$	C11 (2*a*)	0	0.766	0.832
			C12 (2*a*)	0	0.937	0.336
(B2), CaF_2	$Pmc2_1$ (26), orthorhombic	$a = 3.324, b = 4.146, c = 5.686$	Ca (2*a*)	0	0.135	0.703
		$\alpha = 90.00, \beta = 90.00, \gamma = 89.67$	F2 (2*b*)	$\frac{1}{2}$	0.905	0.482
			F1 (2*a*)	0	0.372	0.348
(C5)[a], MgF_2	$C12/c1$ (15), cell choice 1, monoclinic	$a = 5.616, b = 10.351, c = 3.875$	Mg (2*c*)	$\frac{1}{4}$	$\frac{1}{4}$	$\frac{1}{2}$
		$\alpha = 90.00, \beta = 40.31, \gamma = 90.00$	F1 (2*c*)	$\frac{3}{4}$	$\frac{1}{4}$	$\frac{1}{2}$
			F2 (2*b*)	$\frac{1}{4}$	$\frac{1}{4}$	0
(C2), MgF_2	$P4/nmm$ (129), orig. choice 2, tetragonal	$a = 4.060, b = 4.060, c = 3.820$	Mg (4*e*)	0	0.376	$\frac{1}{4}$
		$\alpha = 90.00, \beta = 90.00, \gamma = 90.00$	F1 (4*e*)	0	0.596	$\frac{1}{4}$
			F2 (4*e*)	0	0.624	$\frac{1}{4}$
(D1), MgF_2	$Amm2$ (38), orthorhombic	$a = 3.551, b = 3.155, c = 5.540$	Mg (2*b*)	$\frac{1}{2}$	0	0.069
		$\alpha = 90.00, \beta = 90.00, \gamma = 90.00$	F1 (4*d*)	0	0	0.568
			F2 (2*b*)	$\frac{1}{2}$	0.500	0.738
(D2), MgF_2	$P\bar{1}$ (2), monoclinic	$a = 5.949, b = 5.224, c = 4.004$	Mg (2*i*)	0.661	0.626	0.892
		$\alpha = 90.00, \beta = 90.00, \gamma = 90.00$	F1 (2*i*)	0.378	0.426	0.653
			F2 (1*d*)	$\frac{1}{2}$	$\frac{1}{2}$	0
			F3 (1*c*)	0	0	0
(E1), $MgCl_2$	$Pmma$ (51), orthorhombic	$a = 7.475, b = 3.987, c = 4.890$	Mg (2*a*)	0	0	0
		$\alpha = 90.00, \beta = 90.00, \gamma = 90.00$	C11 (2*f*)	$\frac{1}{4}$	$\frac{1}{2}$	0.447
			C12 (2*e*)	$\frac{1}{4}$	0	0.245
(E2), $MgCl_2$	$P\bar{4}m2$ (115), tetragonal	$a = 4.060, b = 4.060, c = 4.188$	Mg (1*b*)	$\frac{1}{2}$	$\frac{1}{2}$	0
		$\alpha = 90.00, \beta = 90.00, \gamma = 90.00$	Cl (2*g*)	0	$\frac{1}{2}$	0.228
(E3), $MgCl_2$	$P\bar{1}$ (2), monoclinic	$a = 6.695, b = 7.663, c = 6.084$	Mg (2*i*)	0.852	0.863	0.476
		$\alpha = 103.53, \beta = 95.05, \gamma = 67.51$	C11 (1*g*)	0	$\frac{1}{2}$	$\frac{1}{2}$
			C12 (1*f*)	$\frac{1}{2}$	0	$\frac{1}{2}$
(E4), $MgCl_2$	$Ama2$ (40), orthorhombic	$a = 7.317, b = 6.006, c = 6.038$	Mg (4*b*)	$\frac{1}{4}$	0.993	0.949
		$\alpha = 90.00, \beta = 90.00, \gamma = 90.00$	C11 (4*b*)	$\frac{1}{4}$	0.165	0.426
			C1 (4*a*)	0	0	0.277

[a] Anatase-like structure.

halogenides and oxide hydroxides (28), the prism caps are formed by atoms on the prism edge of opposite monocapped prisms that are opposite to the caps instead of neighboring prisms as for example in baddeleyit ZrO_2 (28).

The prism structure C4 found in the MgF_2 and $CaCl_2$ systems consists of edge- and corner-connected trigonal prisms. In this case, however, the prisms do not form a layer as in MoS_2 (28) but rather a three-dimensional network by inserting every second prismatically coordinated cation into the plane between the layers. In addition to these minima, the octahedral coordination of the anatase structure has also been found for $\varepsilon = 0.1$ and $\varepsilon = 0.4$ in the case of MgF_2 (listed as C5).

Another structure with octahedral coordination is C2 (see Fig. 2). This structure is constructed from layers of edge-connected octahedra that are connected by the vertex atoms of the octahedra. The arrangement can be described as a cubic close packing of anions with half of the octahedral sites filled by the cations. This corresponds to a pseudolayer structure of half-filled NaCl. This ion arrangement could be stable in systems where a tetragonal planar arrangement is preferred, for example in systems containing ions with a d^8 electron configuration (29).

Fivefold coordination is observed in structures with trigonal bipyramids as coordination polyhedra. The D1 structure is analogous to a local minimum found in simulated annealing runs for NaCl consisting of trigonal bipyramids (18). In D1 half of these sites are filled whereas D2 forms edge-connected rings of chains of alternating trigonal bipyramids.

The fourfold coordination is only observed in the system $MgCl_2$. In the minima E1 to E4 tetrahedra are the building

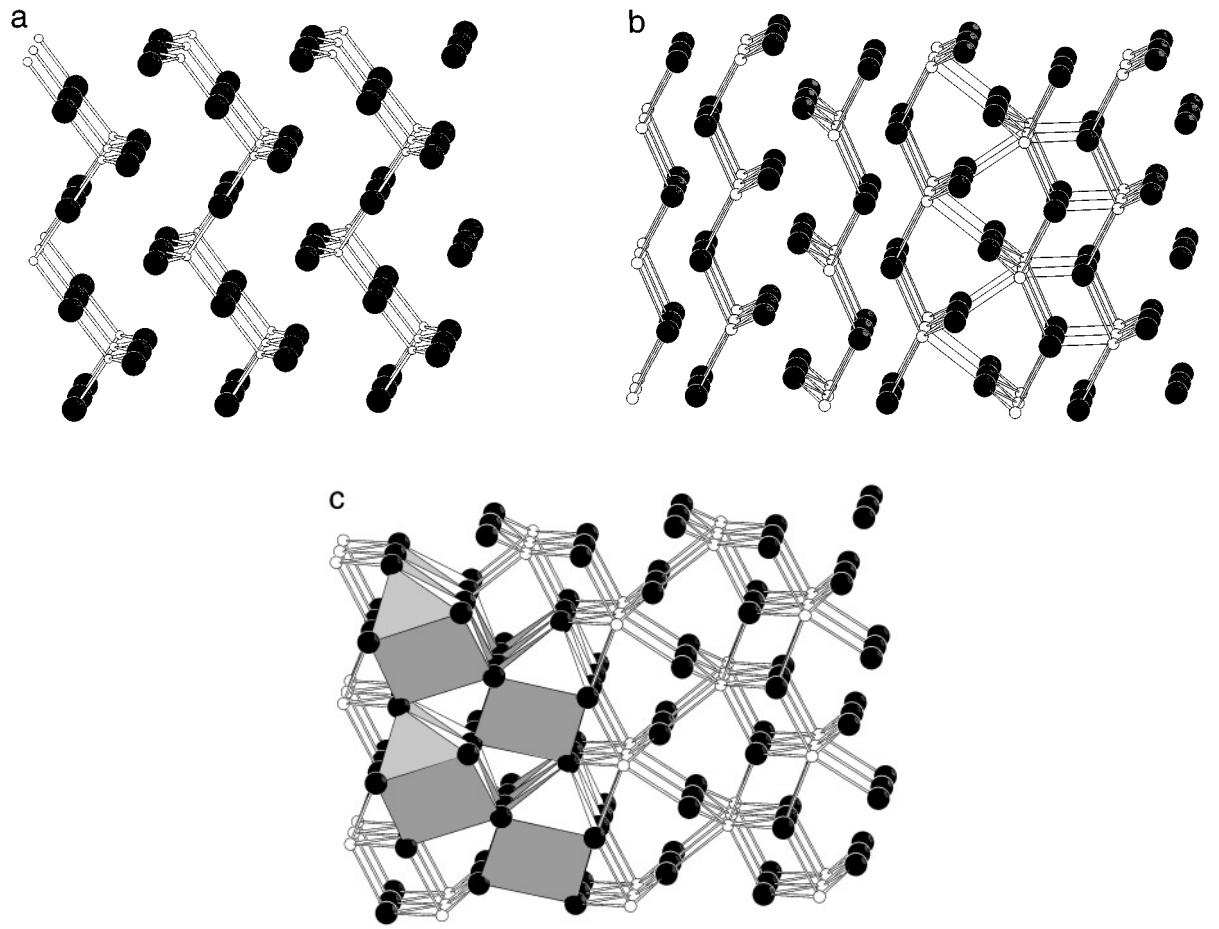

FIG. 1. Ball-and-stick representations of the fourfold-coordinated E1 structure (from $MgCl_2$ runs, shown in (a)) and sevenfold-coordinated B1 structure (from $CaCl_2$ runs, shown in (c)) with some of the coordination polyhedra about the cations (small balls) drawn. A slightly distorted version of the B1 minimum structure is shown in (b), where some of the three longer cation–anion distances have been drawn as lines. Note that the B1 structure forms a 'backbone' that is nearly congruent with the E1 structure motive.

units of layer structures. Comparison with configurations with higher coordination numbers suggests a character of intermediate minima. The energy barrier is probably not very high and may be easily crossed during most of the simulated annealing runs.

The structure E1 was also observed as an intermediate configuration in simulated annealing runs for the TiO_2 system by Freeman and Catlow (30). Thus, the structures with lower coordination numbers (CN = 4 and 5) are presumably the least important ones and are therefore not included in most of the further discussion, with the exception of the $MgCl_2$ system.

4.3. Energy

The minimal energies of the main structure types for each value of ε are listed in Table 4. The general dependence on the Lennard-Jones parameter ε is shown as a typical example for the rutile structure in Fig. 3. For a certain value of ε there exists a maximum in the energy of the configuration. This is in agreement with the general properties of the potential employed (18). For each system the energetic order of the particular minima is independent of the Lennard-Jones parameter (see Table 4). The low-coordinated structures (four- and fivefold) are highest in energy. The layer structure CdI_2 is energetically higher than the pseudolayer structure ccp, $\frac{1}{2}$O. This is probably due to the less favorable Coulomb type interaction within the layers in the CdI_2 type. A β modification of $MgCl_2$ that crystallizes in a CdI_2 structure type has been reported to exist (31).

The structures of the energetically best minima correspond to the experimentally observed crystal structure, except for the layer structure of $MgCl_2$. This system produces a rutile minimum as the energetically best one. To test

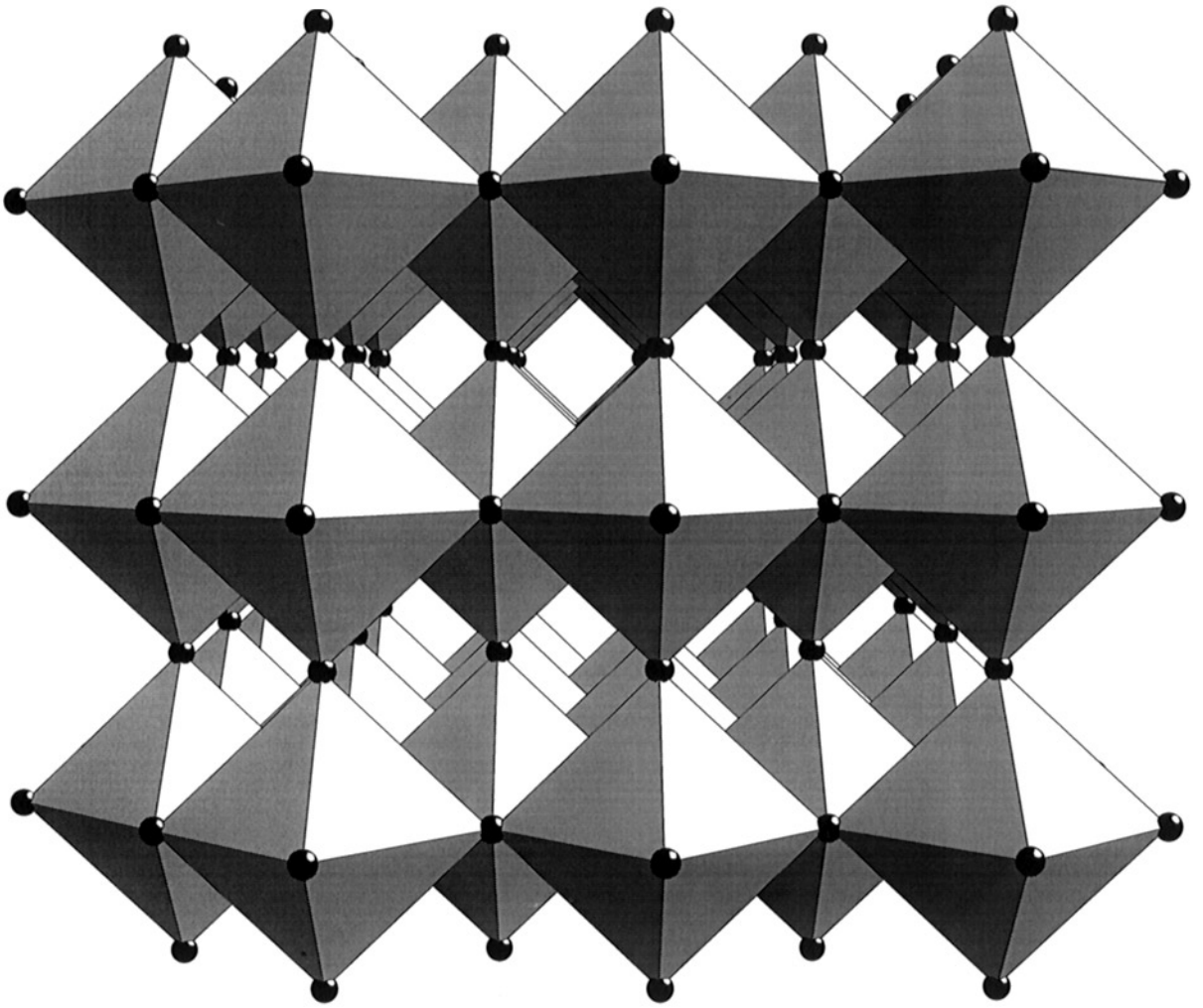

FIG. 2. Structure of the C2 minimum (half-filled NaCl type): corner-connected layers of edge-connected octahedra of AB_6 units (A = Mg, Ca; B = F, Cl).

whether the real structure of $MgCl_2$ corresponds to a local minimum of the energy function, this ion arrangement (rhombohedral unit cell, doubled in the [100] direction) was used as a starting configuration for quench runs with 10 000 steps. To check the robustness of this minimum with respect to the strength of the Lennard-Jones potential term, ε was varied between 0.05 and 1.0. The results are listed in Table 5. The $CdCl_2$-type minimum is kinetically stable for $\varepsilon \geq 0.1$, but it is not the absolute minimum of the energy landscape. The quench for $\varepsilon = 0.05$ ends in the structure E1 with tetrahedral coordination. Ion arrangements with layer structures seem to be preferred when the van der Waals term becomes more important, whereas the lower coordination is achieved by increasing the relative importance of the Coulomb part in the potential. It should be noted that the calculated real layer structure is higher in energy than the other sixfold-coordinated minimum structures found in the $MgCl_2$ system (cf. Tables 4 and 5). This result agrees with studies by Busing (32), who observed that in the case of magnesium chloride the hypothetical rutile-like structure calculated with a Born–Meyer potential (33) was lower in energy compared with the same energy calculation of the real crystal structure. The recalculation with an adjustment of the potential to a nonspherical chloride ion and the use of higher multipole terms was also found to be insufficient to correctly predict the energy of the crystal structure of $MgCl_2$ ($CdCl_2$ type) relative to the rutile structure (32).

4.4. Cation–Anion Distance

The distances between anions and cations strongly depend on the value of ε. In Table 6 the results for the most common structures with low energies are summarized.

TABLE 4
Minimal Energies of the Main Minima for the AB_2 Systems MgF_2, $MgCl_2$, CaF_2, and $CaCl_2$ ($Z = 2$), with Fivefold and Fourfold Coordination Included for Comparison

$\varepsilon(Mg_2F_4)$ (eV/atom)	CaF_2 (A1)	MP1 (B1)	Rutile (C1)	ccp, $\frac{1}{2}$ O (C2)	CdI_2 (C3)	Anatase (C5)	CN = 5 (D1, D2)	CN = 4 (E1–E4)
0.1			− 6.679	− 6.320[b]	− 6.270	− 6.544[b]	− 6.286	
0.2		− 6.152	− 6.398	− 6.056	− 5.986		− 5.907	
0.3		− 6.118	− 6.346	− 6.030	− 5.931		− 5.767	
0.4		− 6.168	− 6.376	− 6.030[b]	− 5.960	− 6.200[b]		
0.5		− 6.258	− 6.449	− 6.130[b]	− 6.030			
$\varepsilon(Mg_2Cl_4)$ (eV/atom)	CaF_2 (A1)	MP1 (B1)	rutile (C1)	ccp, $\frac{1}{2}$ O (C2)	CdI_2 (C3)	anatase (C5)	CN = 5 (D1, D2)	CN = 4 (E1–E4)
0.1			− 4.109		(− 3.741)[a]			− 4.022
0.2			− 3.989		− 3.603			− 3.783
0.3			− 4.030	− 3.813	− 3.630[b]		− 3.694	− 3.744
0.4			− 4.129	− 3.917	− 3.718[b]			− 3.255
0.5			− 4.256	− 4.050	− 3.835[b]			− 4.039
$\varepsilon(Ca_2F_4)$ (eV/atom)	CaF_2 (A1)	MP1 (B1)	rutile (C1)	ccp, $\frac{1}{2}$ O (C2)	CdI_2 (C3)	anatase (C5)	CN = 5 (D1, D2)	CN = 4 (E1–E4)
0.1	− 7.054		− 6.934		− 6.702			
0.2	− 6.832	− 6.502[b]	− 6.642		− 6.446[b]			
0.3	− 6.810	− 6.472						
0.4	− 6.860							
0.5	− 6.945		− 6.599					
$\varepsilon(Ca_2Cl_4)$ (eV/atom)	CaF_2 (A1)	MP1 (B1)	rutile (C1)	ccp, 1/2 O (C2)	CdI_2 (C3)	anatase (C5)	CN = 5 (D1, D2)	CN = 4 (E1–E4)
0.1		− 4.925	− 5.113		− 4.811			
0.2		− 4.808	− 4.981	− 4.747	− 4.676			
0.3		− 4.850[b]	− 5.004	− 4.782	− 4.698			
0.4		− 4.948	− 5.084	− 4.870	− 4.775			
0.5			− 5.192					

[a] This is the result of a quench run starting with $MgCl_2$ in a CdI_2 structure.
[b] These structures appeared only once as minima during the simulated annealing runs.

This parameter dependence is a general property of the potential (18). Increasing the ε parameter results in a stronger influence of the repulsive forces (and the van der Waals attraction) of the ions in the Lennard-Jones potential. For the same ion arrangement the distances are balanced by the repulsive forces, increasing the cation–anion and anion–anion distances for larger values of ε. The distance dependence on ε for the most important minima is plotted in Fig. 4 for the main sixfold-coordinated structures (eightfold in the case of the CaF_2 system). The approximate ion separation in the real compound is depicted as a dashed line. The ε values where the shortest cation–anion distances in the simulated structures of the different systems agree best with those in the real crystals are 0.3 (MgF_2), < 0.1 ($MgCl_2$), 0.4–0.5 (CaF_2), and 0.3 ($CaCl_2$).

4.5. Angle Distortion in the Rutile-Type Structure to the $CaCl_2$ Structure

If one considers the rutile minima in the three systems MgF_2, $MgCl_2$, and $CaCl_2$, a slight distortion in the angle φ between the octahedra of edge-connected chains is observed (see Table 7). A distortion angle $\varphi_{real} = 12.58^\circ$ corresponds to the real $CaCl_2$ crystal structure as a variant of the rutile type (34). Further distortion of φ results in a hexagonal close packing of anions (see Fig. 5). The ε dependence of φ for the systems under consideration is shown in Fig. 6. It is obvious that for MgF_2 φ is always considerably smaller than the angle for $CaCl_2$, in agreement with the experimentally found structures. The distortion angle observed in crystals of $CaCl_2$ is best approximated at about $\varepsilon = 0.4$,

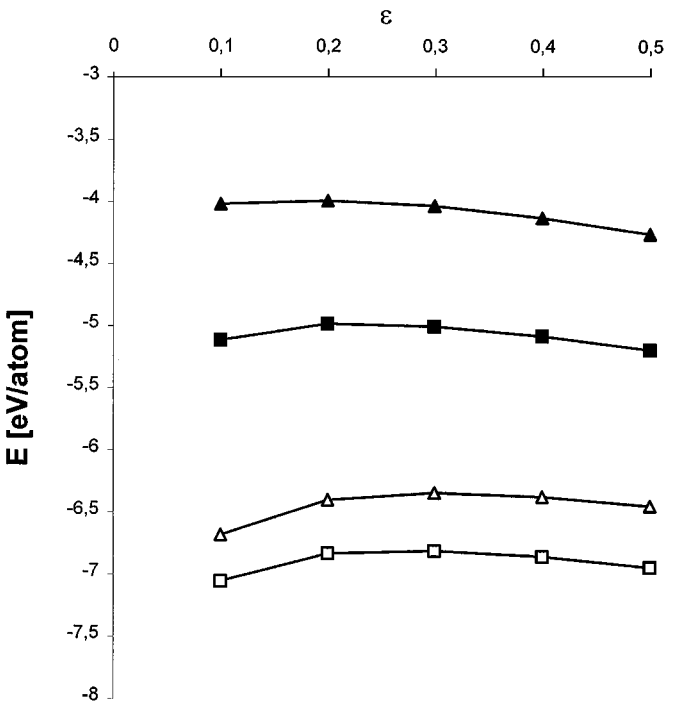

FIG. 3. Energy of rutile-like minima (fluorite minimum for CaF_2) as a function of ε ((△) MgF_2, (▲) $MgCl_2$, (□) CaF_2, (■) $CaCl_2$).

whereas an angle distortion for MgF_2 is significant for $\varepsilon > 0.3$ only. For $CaCl_2$ this value differs from the ε value for the best distance approximation (see Section 4.4). Apparently, structural details such as angles and distances can be predicted only approximately, but general features such as coordination, connection between the polyhedra, and tendencies in the structure deformation for different ions are correctly represented by the potential.

5. DISCUSSION

The calculations in the AB_2 systems show that structure prediction for ionic systems with no more information than composition and ion types is (in principle) possible using global optimization to determine possible structure candidates. As mentioned in the introduction, these have to be investigated further with regard to their stability. We are currently investigating this question following a general procedure that has been described elsewhere (3, 8).

When discussing the results of the simulated annealing, we need to consider several aspects separately: first, the configuration space that is investigated during the optimization; second, the detailed properties of the potential employed; and third, the generality and transferability of the energy landscape.

TABLE 5
Quench Runs (10 000 Optimization Steps) for $MgCl_2$[a]

$\varepsilon(MgCl_2)$	E (initial)	E (final)	d_{Mg-Cl} (Å)
(0.05)[b]	(− 3.638)	(− 4.341)	(2.14)
0.1	− 3.532	− 3.739	2.39
0.2	− 2.519	− 3.467	2.44
0.3	− 1.506	− 3.345	2.47
0.4	− 0.493	− 3.282	2.49
0.5	0.52	− 3.247	2.51
1.0	+ 5.585	− 3.235	2.54

[a] Start configuration is $MgCl_2$ in the real crystal structure ($CdCl_2$ type). Initial and final energies are given in eV/atom, and the range of ε values is extended to 0.05–1.0. The Mg–Cl distance is listed in the last column.

[b] The run for $\varepsilon = 0.05$ results in an E1-minimum with a fourfold coordination.

TABLE 6
Mean Distances $d_{cation-anion}$ for the Main Sixfold-Coordinated Structures (Eightfold in the Case of CaF_2) for Different ε Values

	d_{Mg-F} (Å)				
	$\varepsilon = 0.1$	$\varepsilon = 0.2$	$\varepsilon = 0.3$	$\varepsilon = 0.4$	$\varepsilon = 0.5$
CdI_2	1.86	1.95	2.00	2.04	2.06
ccp, $\frac{1}{2}$O	1.86[a]	1.94	1.95	2.02[a]	2.05[a]
rutile	1.84	1.93	1.98	2.01	2.04
Mp1		2.07	2.18	2.12	2.14
	d_{Mg-Cl} (Å)				
	$\varepsilon = 0.1$	$\varepsilon = 0.2$	$\varepsilon = 0.3$	$\varepsilon = 0.4$	$\varepsilon = 0.5$
CdI_2		2.53	2.59[a]	2.62[a]	2.65[a]
ccp, $\frac{1}{2}$O			2.60	2.64	2.66
rutile	2.41	2.52	2.57	2.61	2.64
	d_{Ca-F} (Å)				
	$\varepsilon = 0.1$	$\varepsilon = 0.2$	$\varepsilon = 0.3$	$\varepsilon = 0.4$	$\varepsilon = 0.5$
CdI_2	2.08	2.19[a]			
rutile	2.06	2.17			2.33
Mp1		2.21[a]	2.30	2.30	2.34
CaF_2	2.15	2.25	2.31	2.35	2.37
	d_{Ca-Cl} (Å)				
	$\varepsilon = 0.1$	$\varepsilon = 0.2$	$\varepsilon = 0.3$	$\varepsilon = 0.4$	$\varepsilon = 0.5$
CdI_2	2.58	2.71	2.78	2.82	
ccp, $\frac{1}{2}$O		2.69	2.75	2.79	2.82
$CaCl_2$ (hcp)	2.56	2.68	2.74	2.78	2.81
Mp1	2.53	2.84	2.89[a]	2.93	2.95

[a] These structures appeared only once as minima during the simulated annealing runs.

5.1. *Aspects of the Optimization Concerning the Accessible Configuration Space*

The optimization parameters and the temperature schedule were taken from previous works (7, 18, 26). However, the

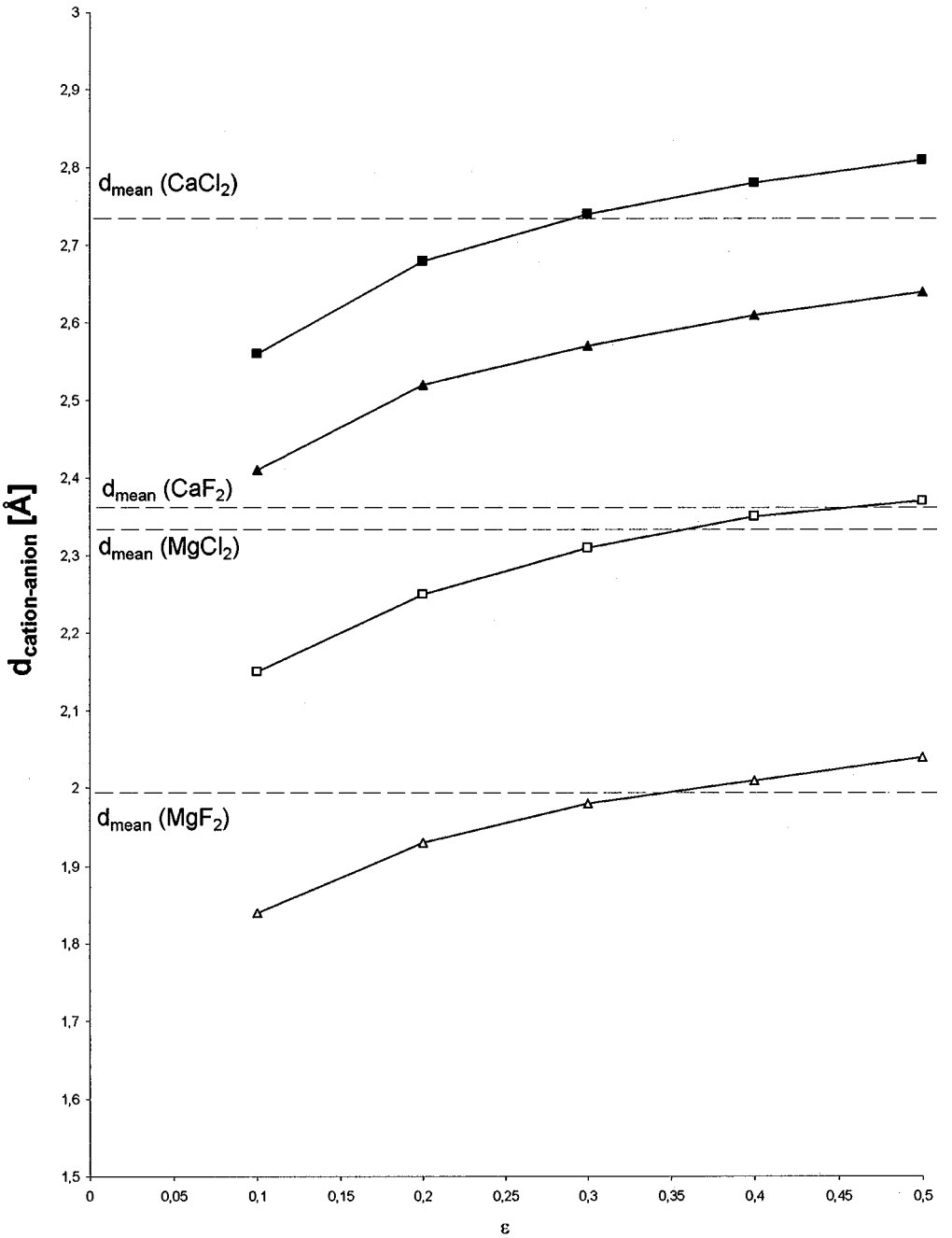

FIG. 4. Cation–anion distance for rutile-like minima (fluorite minimum for CaF_2), as a function of ε. ((△) MgF_2, (▲) $MgCl_2$, (□) CaF_2, (■) $CaCl_2$). The dashed lines correspond approximately to d_{mean} from crystal structure measurements for each compound (see Table 1). The intersection gives a possible criterion for optimal values of ε. It is to be noted that the dashed line for $MgCl_2$ is the distance in the $CdCl_2$-type structure. This distance does not coincide with any rutile analogue found in the simulation for $MgCl_2$.

choice of the parameters for the optimization procedure depends on the size of the system being studied. The move class limits the accessible configurations in the configuration space. To find the global minimum and the most important energetically low local minima, the move class and the temperature schedule must be chosen in such a way that most of the configuration space can be reached during the simulated annealing. The size of the configuration space is determined by the number of atoms in the optimization cell. Only those structures with no more than N atoms in the smallest possible unit cell can occur as local minima on the energy hypersurface. Likewise the total number of steps

TABLE 7
Distortion Angle φ (Deg) in the Rutile-like Minima in MgF_2, $MgCl_2$, and $CaCl_2$ Depending on ε

	$\varepsilon = 0.1$	$\varepsilon = 0.2$	$\varepsilon = 0.3$	$\varepsilon = 0.4$	$\varepsilon = 0.5$
MgF_2	0.49	0.8	3.02	8.87	12.48
$MgCl_2$	0.14	1.06	2.27	4.42	9.66
$CaCl_2$	1.00	2.72	8.62	11.95	15.19

must be adjusted so that the percentage of moves per atom is about the same as for fewer atoms per cell.

Calculations with 12 atoms ($Z = 4$) for MgF_2, $MgCl_2$, and $CaCl_2$ show that the rutile structure is also present in the larger system and that this minimum remains the one with the lowest energy. Further results obtained from these runs comprise new local minima with reasonable structures (20). The most important new minimum is the α-PbO_2 structure, which is energetically nearly equal to the rutile minimum. This structure is experimentally found as a high-pressure modification in titanium dioxide (35) and many other compounds (28). In addition, an analogue of the Li_2ZrF_6 structure type (28) is observed where Li and Zr are replaced by the cation Mg^{2+}. Catlow *et al.* also found a minimum with an α-PbO_2 structure that has a comparatively low energy like the rutile minimum in simulated annealing studies of TiO_2 using crystallographic cell data (36).

The fact that the real structures, for both $Z = 2$ and $Z = 4$, correspond to the energetically lowest minima supports the thesis that the simulated annealing algorithm is able to find the important local minima (i.e., real crystal

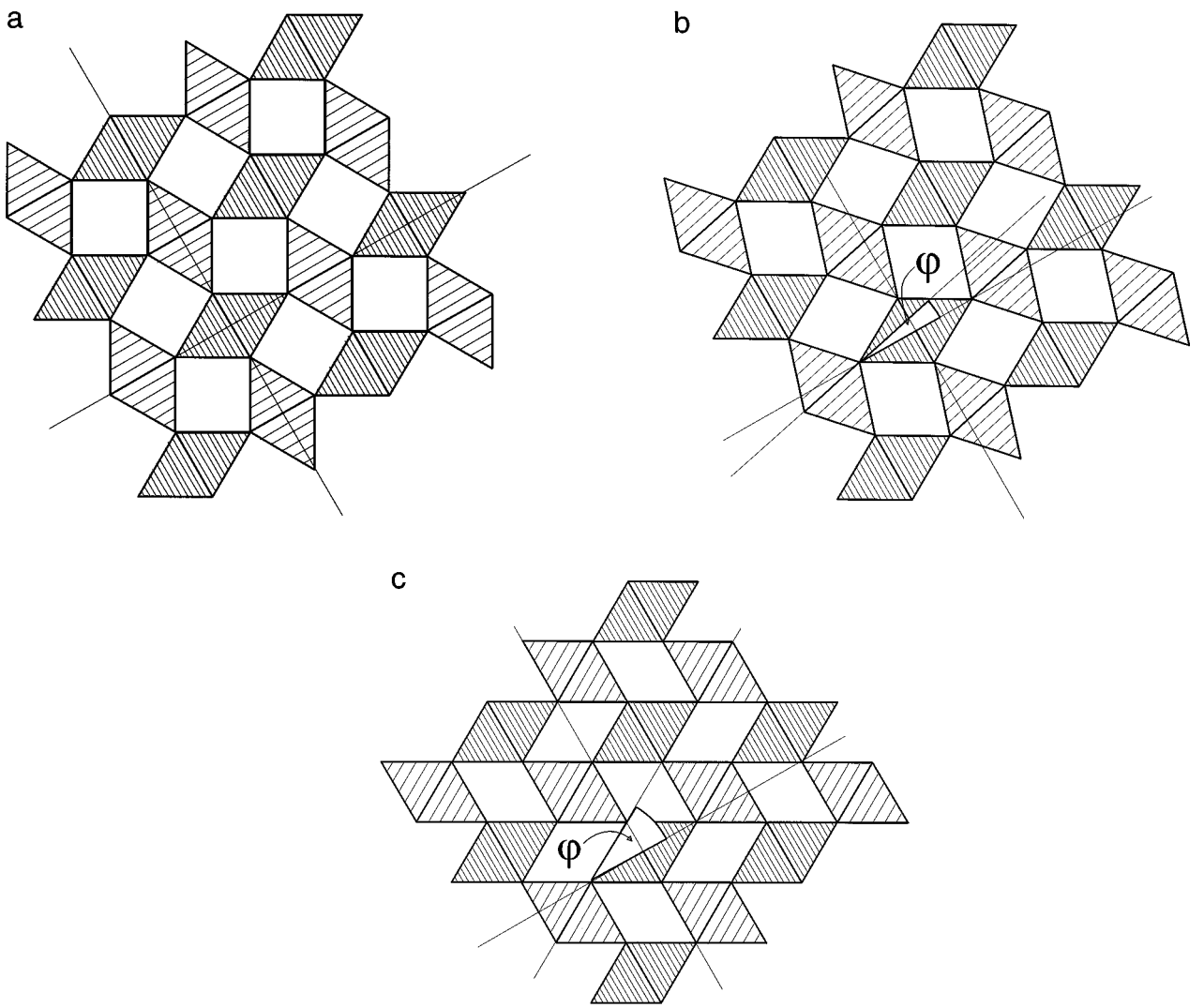

FIG. 5. Topological transition from rutile (a) to hexagonal close packing (hcp) (c) with half-filled octahedral sites (schematically). The distortion angle between chains of octahedra is φ. The $CaCl_2$ structure (b) is an intermediate structure with $\varphi_{real} = 12.58°$.

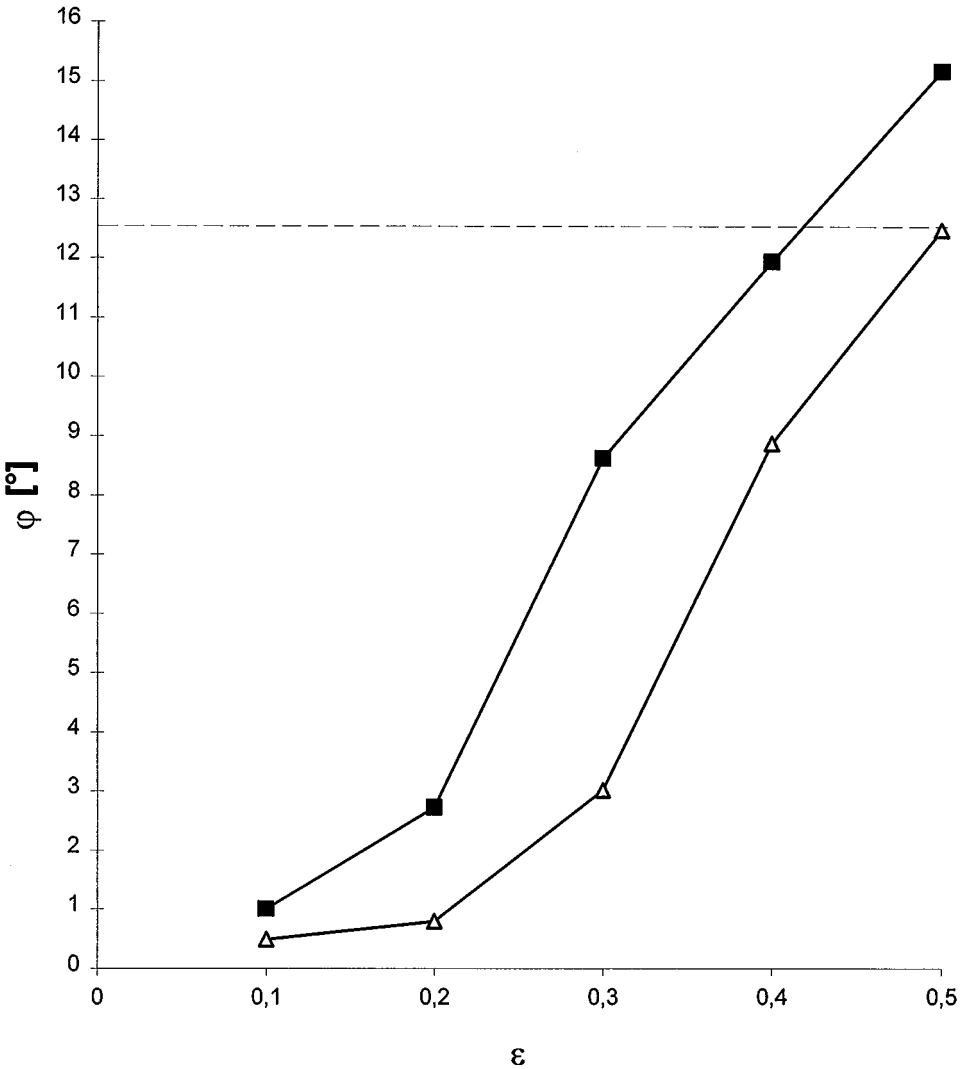

FIG. 6. Mean distortion angle in the rutile-like structures for the transition to the $CaCl_2$ type as a function of ε. ((△) MgF_2, (■) $CaCl_2$). The dashed line marks $\varphi_{real} = 12.58°$.

structures and their respective modifications) on the potential energy surface with the temperature schedule and move class used. For larger systems, though, the number of minima grows considerably, requiring a larger number of runs to have a relatively complete representation of the configuration space.

5.2. General Properties of the Potential

The energy in the potential employed in this research is controlled by two main terms: the Coulomb term, with about 90% of the total energy, and the repulsive force r^{-12} term, modified by the attractive van der Waals r^{-6} term. For the Coulomb term the contribution rises with charge and reciprocal distance. The strength of the repulsion due to the r^{-12} term is controlled by the Lennard-Jones parameter ε, which represents the hardness of the ions. For constant distance the repulsion increases linearly with ε (18).

The number of terms with positive or negative contributions, representing attractive or repulsive interactions, and the size of these contributions are in balance for a specific energy of a configuration. This has consequences for the structure–energy relations of a configuration, i.e., the way the energy is changed when the geometrical arrangement of the ions is altered. One example is the resulting coordination sphere about the cations in the minimum structures in an optimization. If the difference in the energy contribution of positive and negative interactions is not very large, it is normally preferable to arrange more anions around cations depending on the prescribed radius of the cation. Otherwise, if the repulsion between these anions is large

enough (i.e., large ε), they will likely shift to another arrangement with a lower total energy, where the high positive energies are reduced by either an enlarged distance or a smaller number of such contributions. In addition, combinations of these two alternatives are possible as well. This balance of the size and number of attractive and repulsive terms can be perturbed even by minor energy terms and result in an alternate ion arrangement if the number of ions with specific small contributions (e.g., greater distance) becomes large enough by the structural change (for instance more ions in the second coordination sphere) and if this is not canceled by other interactions with considerably large contributions. Since this may lead to high energy barriers for certain small structural changes, it is not a viable strategy to start the simulated annealing runs using only known structure types as initial configurations to find new promising structure candidates. For example, if one had followed such a strategy, the structure C2 would most likely not have been encountered. This also explains why no distinct tendency in AB_2 systems for the occurrence of a special coordination number depending on ε can be observed. Likewise the influence on the energy landscape of refining the potential by introducing additional energy terms cannot be predicted straightforwardly, even if these terms are only small contributions.

From this brief discussion it should be obvious that the energy of any structure requires consideration of all ion interactions described by the potential that have a significant contribution. The decision whether a term is significant or not is not trivial, because the number of such contributions is often at least as important as the size of the interaction.

5.3. *Transferability and Generality of the Potential*

The empirical potential used in this work has been chosen as the energy function for the advantage of being fast to calculate at low computational cost. As a consequence the calculated energies for real structures may differ from experimental values. On the other hand, improvements beyond the ionic model, for example with polarizable ions, have the disadvantage of introducing additional adjustable parameters. Such potentials are often used when the potential parameters can be fitted to real crystal properties (37, 38). However, the results in this work show that the Lennard-Jones parameter can be varied over a considerably wide range ($0.1 < \varepsilon < 0.5$) while preserving most of the general characteristics of the energy landscape, i.e., the structural characteristics of the minima and their relative energies. The variation of these parameters rather affects structural details such as distances and angles.

Another advantage of using general parameter values is the fact that they remain approximately valid over a relatively large region of configuration space. Parameters fitted to experiments are often only suitable for the structural minimum they are derived from (38). However, during a global optimization structures with many different coordination numbers and large variations of nearest-neighbor distances are frequently encountered. Therefore, the use of a potential that is also appropriate for these configurations is essential.

As pointed out before, the general form of our empirical potential is a combined Coulomb and Lennard-Jones potential. In addition to the Lennard-Jones parameter ε the potential parameters are the ion charge and ionic radii. The formal ion charge and the ionic radii, which are a compromise for different coordinations, are approximate parameter values, but reasonably chosen considering the chemical model that is the basis for this potential. Changing the charge or the radii arbitrarily corresponds to a hypothetical adjustment of the chemical characteristics of the AB_2 compound. Therefore it should be possible to find the minimum structures in other chemical compounds besides the particular AB_2 system where the configuration was observed. For example, the CdI_2 minimum exists as a structure type for many AB_2 compounds. Likewise the octahedrally coordinated C2 minimum (NaCl with half-filled octahedral sites) could be a possible structure candidate in AB_2 systems.

Considering these aspects and the results in this work, the energy landscape constructed from the potential and a particular choice of parameter values should be regarded as a representative for a given class of chemical systems. The quality of this representation depends on the possibility to predict the real crystal structures. Further tests of this method for constructing an energy hypersurface for a real chemical compound should involve systems with many structural modifications that can be represented by the same empirical potential model[5] (38).

6. SUMMARY

We have shown that structure prediction using empirical potentials and simulated annealing as a global optimization method is possible as long as the potential is a good representative for the chemical system under study. The resulting minima may be interpreted as structure candidates for the crystalline compound. The subsequent stability analysis of these structure candidates and the extension to $T \neq 0\,\mathrm{K}$ require a very high amount of further computational effort. However, the simulated annealing algorithm alone already produces minima with low relative energies that often correspond to structures of real crystalline compounds. The studies of simple ionic systems are encouraging with respect

[5]It is to be expected that with future development in computer techniques the use of more sophisticated energy calculation methods such as the LDA (5) or Hartree–Fock (6) is imminent.

to the extension of this method to the prediction of hitherto unknown compounds. The first applications of this method to determine structure candidates and possible stable modifications of not-yet-synthesized compounds are studies of noble gas crystals (7, 9), alkali-metal nitrides (39, 40), and the system Ca_3SiBr_2 (41).

REFERENCES

1. "Structure and Bonding in Crystals" (M. O'Keefe and A. Navrotsky, Eds.), Vols. I and II. Academic Press, London, 1981.
2. M. Jansen, "Wege zu Festkörpern jenseits der thermodynamischen Stabilität," *in* Nordrhein.-Westfael. Akad. Wiss, Vorträge No. 420 (1996).
3. J. C. Schön and M. Jansen, *Angew. Chem., Int. Ed. Engl.* **35,** 4001 (1996).
4. J.-R. Hill and J. Sauer, *J. Phys. Chem.* **98,** 1238 (1994).
5. W. Kohn and L. J. Sham, *Phys. Rev. A* **140,** 113 (1965).
6. C. Pisani, R. Dovesi, R. Nada, and L. N. Kantorovich, *J. Chem. Phys.* **92,** 7448 (1988).
7. H. Putz, J. C. Schön, and M. Jansen, *Ber. Bunsenges. Phys. Chem.* **99,** 1148 (1995).
8. J. C. Schön and M. Jansen, *in* "Pauling's Legacy: Modern Modelling of the Chemical Bond" (Z. B. Maksic and W. J. Orville-Thomas, Eds.), Elsevier, New York, 1998, in press.
9. J. C. Schön, H. Putz, and M. Jansen, *J. Phys: Condens. Mater.* **8,** 143 (1996).
10. J. C. Schön, *Ber. Bunsenges. Phys. Chem.* **9,** 1388 (1996).
11. J. Pannetier, J. Bassas-Alsina, J. Rodriguez-Carvajal, and V. Caignaert, *Nature* **346,** 343 (1990).
12. M. W. Deem and J. M. Newsam, *J. Am. Chem. Soc.* **114,** 7189 (1989).
13. C. R. A. Catlow, A. N. Cormack, and F. Theobald, *Acta Crystallogr., Sect. B* **40,** 195 (1984).
14. M. W. Deem and J. M. Newsam, *Nature* **342,** 260 (1989).
15. C. M. Freeman, J. M. Newsam, S. M. Levine, and C. R. A. Catlow, *J. Mater. Chem.* **3,** 531 (1993).
16. R. G. Bell, R. A. Jackson, and C. R. A Catlow, *J. Chem. Soc., Chem. Commun.* 782 (1990).
17. C. R. A. Catlow and G. D. Price, *Nature* **347,** 243 (1990).
18. J. C. Schön and M. Jansen, *Comput. Mater. Sci.* **4,** 43 (1995).
19. S. W. De Leeuw, J. W. Perram, and E. R. Smith, *Proc. R. Soc. London, A* **373,** 27 (1980).
20. M. Wevers, Diploma Thesis, University of Bonn, 1994.
21. W. A. Harrison, "Electronic Structure and the Properties of Solids." W. H. Freeman and Co., San Francisco, 1980.
22. J. Emsley, "The Elements." Clarendon Press, Oxford, 1991.
23. S. Kirkpatrick, C. D. Gelatt, Jr., and M. P. Vecchi, *Science* **220,** 671 (1983).
24. N. Metropolis, A. W. Rosenbluth, M. N. Rosenbluth, A. H. Teller, and E. Teller, *J. Chem. Phys.* **21,** 1087 (1953).
25. D. A. Pierre, "Optimization Theory with Applications." Dover Publications, New York, 1986.
26. J. C. Schön and M. Jansen, *Ber. Bunsenges. Phys. Chem.* **12,** 1541 (1994).
27. A. Hannemann, R. Hundt, J. C. Schön, and M. Jansen, *J. Appl. Cryst.* (1998), submitted.
28. B. G. Hyde and S. Anderson, "Inorganic Crystal Structures." John Wiley & Sons, New York, 1989.
29. C. J. Ballhausen, "Introduction to Ligand Field Theory." McGraw-Hill, New York, 1962.
30. C. M. Freeman and C. R. A. Catlow, *J. Chem. Soc., Chem. Commun.* 89 (1992).
31. I. W. Bassi, F. Polato, M. Calcaterra, and J. C. J. Bart, *Z. Kristallogr.* **159,** 297 (1982).
32. W. R. Busing, *Trans. Am. Crystallogr. Assoc.* **6,** 57 (1970).
33. M. Born and J. E. Meyer, *Z. Phys.* **75,** 1 (1932).
34. G. Bergerhoff, R. Hundt, R. Sievers, and I. D. Brown, *J. Chem. Inf. Comput. Sci.* **23,** 66 (1983).
35. P. Y. Simons and F. Dachille, *Acta Crystallogr.* **23,** 334 (1967).
36. C. M. Freeman, J. M. Newsam, and C. R. A. Catlow, *J. Mater. Chem.* **3,** 531 (1993).
37. M. Kunz and T. Armbruster, *Acta Crystallogr., Sect. B* **48,** 609 (1992).
38. T. S. Bush, J. D. Gale, C. R. A. Catlow, and P. D. Battle, *J. Mater. Chem.* **4,** 831 (1994).
39. J. C. Schön, *GIT Fach. Lab.* **1997,** 816 (1997).
40. J. C. Schön and M. Jansen, **624,** 533–540 (1998).
41. H. Putz, J. C. Schön, and M. Jansen, *J. Solid State Chem.* (1998), submitted.